JOURNAL OF SYNCHROTRON RADIATION

Volume 22 (2015)

Supporting information for article:

Indications of radiation damage in ferredoxin microcrystals using high intensity X-FEL beams

Karol Nass, Lutz Foucar, Thomas R. M. Barends, Elisabeth Hartmann, Sabine Botha, Robert L. Shoeman, R. Bruce Doak, Roberto Alonso-Mori, Andrew Aquila, Saša Bajt, Anton Barty, Richard Bean, Kenneth Beyerlein, Maike Bublitz, Nikolaj Drachmann, Jonas Gregersen, H. Olof Jönsson, Wolfgang Kabsch, Stephan Kassemeyer, Jason E. Koglin, Michael Krumrey, Daniel Mattle, Marc Messerschmidt, Poul Nissen, Linda Reinhard, Oleg Sitsel, Dimosthenis Sokaras, Garth J. Williams, Stefan Hau-Riege, Nicusor Timneanu, Carl Caleman, Henry N. Chapman, Sébastien Boutet and Ilme Schlichting

Supporting information

Figure S1 a) Image of the ferredoxin crystal suspension used for the high dose SFX measurements and b) size distributions for the crystal lengths and widths obtained from 222 and 196 measurements respectively. Best fit bell curves (dotted green lines) are displayed, along with the means and standard deviations. Measurements were performed using *AnalyzingDigitalImages* software obtained from: https://sites.google.com/a/globalsystemsscience.org/global-systems-science/software/download

a)

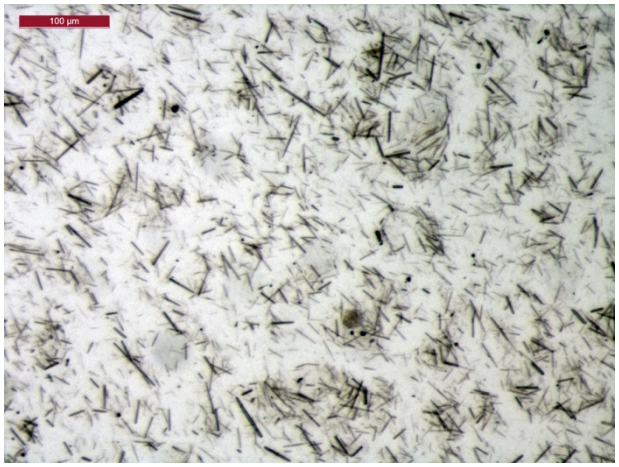

b)

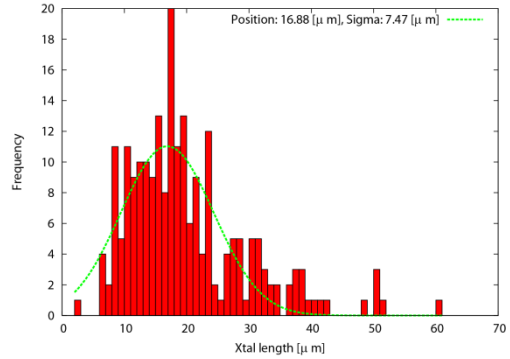

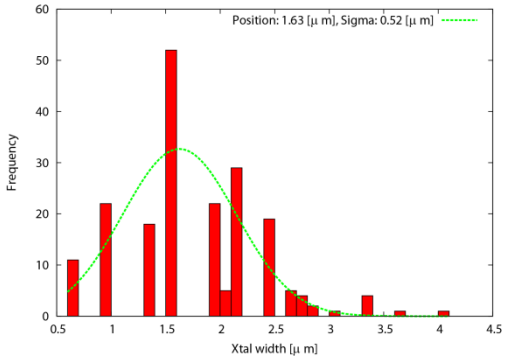

Figure S2 Two coated Kapton films, sandwiched together in a single mount, were used as a post-sample attenuator. These were fabricated in the DESY multilayer optics laboratory by magnetron sputtering through a spinning mask to achieve the desired thickness profile. The coating material was a $W_{0.84}Ta_{0.16}$ alloy with an estimated density of 16 g/cm^3. The filter transmission, as a function of scattering angle, depends on the distance of the source point to the filter, and these were constructed to give constant transmission at a source to filter distance of 1 cm (the sample is the source of the diffracting rays). Here the transmission with a collimated beam is shown at photon energy of 6.8 keV: (a) Transmission in the function of photon energy of the filter with thickness of 5.38 μm in the center (605 in the label) and of the filter with 2.32 μm thickness in the center (606 in the label) at two positions of the filter (center and edge). (b) Measured transmission map of the filter with thickness of 5.38 μm in the center, and (c) transmission map of the filter with 2.32 μm thickness in the center. Measurements were made at the four-crystal monochromator beamline of the Physikalisch-Technische Bundesanstalt at BESSY II where highly monochromatic radiation is available (Krumrey & Ulm, 2001). Insets d, e) show photographs of the filters and transmission profiles measurements at 8.05 keV using laboratory diffractometer before the experiment at LCLS of the same filters as in (a, b, c).

a)

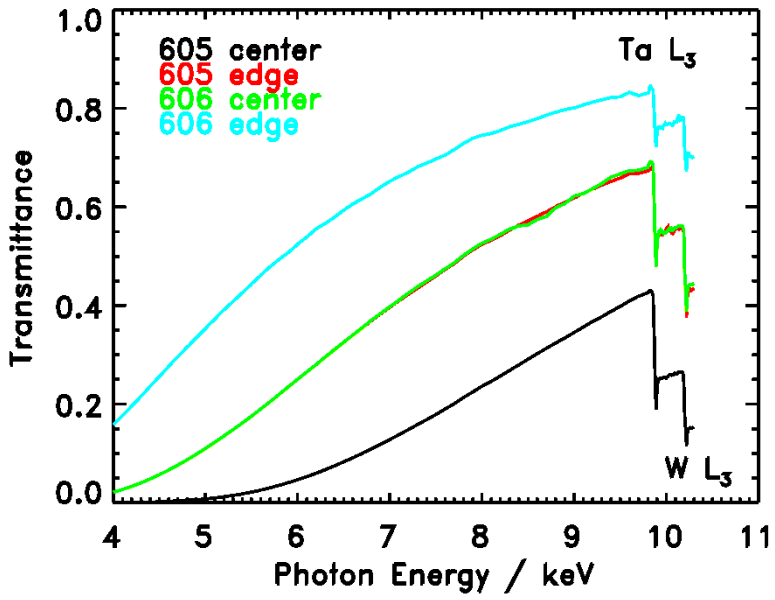

b)

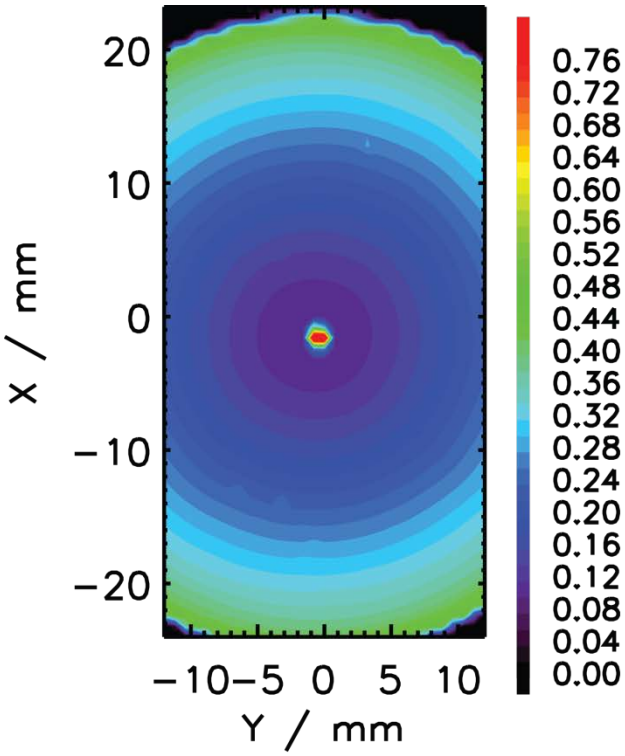
20
10
0
−10
−20
X / mm
−10 −5 0 5 10
Y / mm
0.76
0.72
0.68
0.64
0.60
0.56
0.52
0.48
0.44
0.40
0.36
0.32
0.28
0.24
0.20
0.16
0.12
0.08
0.04
0.00

c)

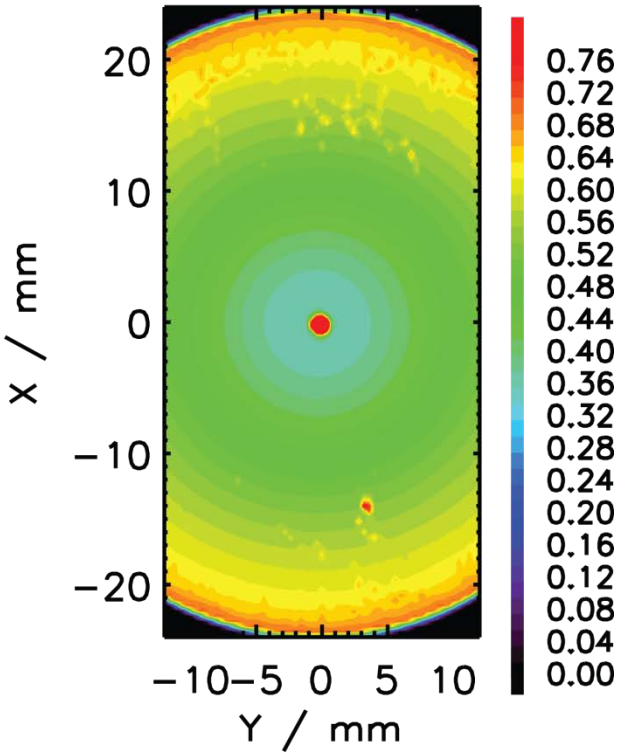
20
10
0
−10
−20
X / mm
−10 −5 0 5 10
Y / mm
0.76
0.72
0.68
0.64
0.60
0.56
0.52
0.48
0.44
0.40
0.36
0.32
0.28
0.24
0.20
0.16
0.12
0.08
0.04
0.00

d)

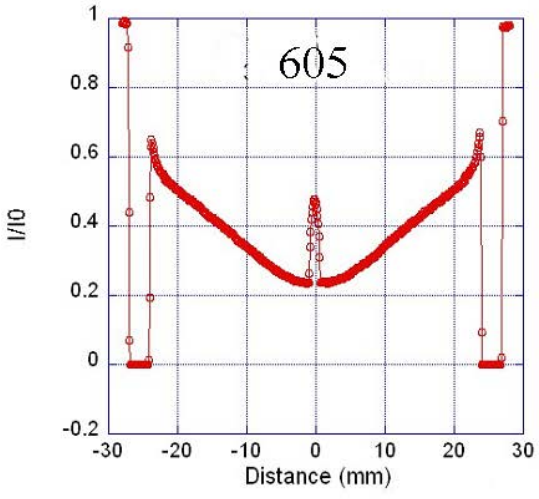
605
I/I0
Distance (mm)
1
0.8
0.6
0.4
0.2
0
-0.2
-30 -20 -10 0 10 20 30

e)

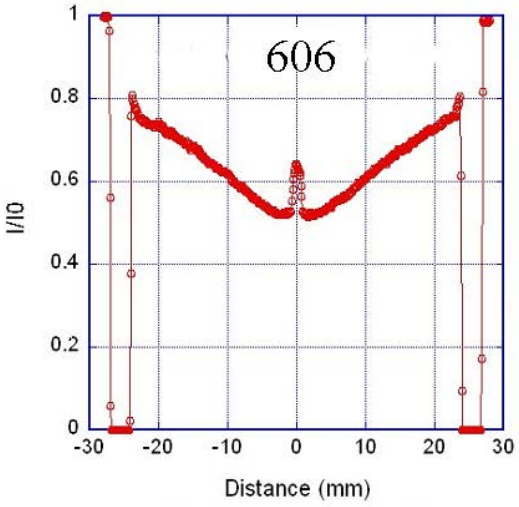
606
I/I0
Distance (mm)
1
0.8
0.6
0.4
0.2
0
-30 -20 -10 0 10 20 30

Figure S3 Distributions of a,b,c unit cell lenghts obtained from the ferredoxin 7.36 keV data set from a subset of 3500 randomly selected images indexed without cell reduction option in CrystFEL.

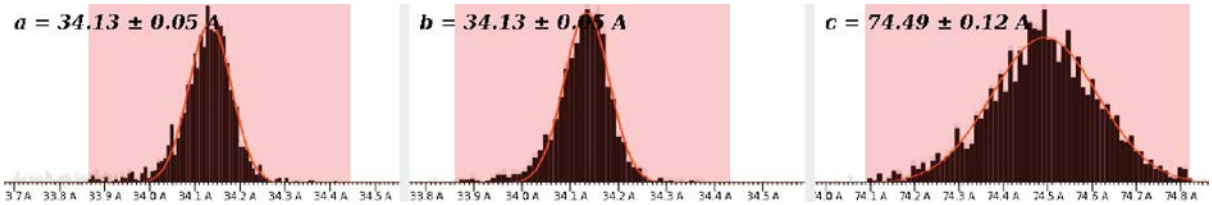

Figure S4 Wilson and cumulative intensity distribution plots for a) high dose LCLS, low dose LCLS and b) SLS data sets.

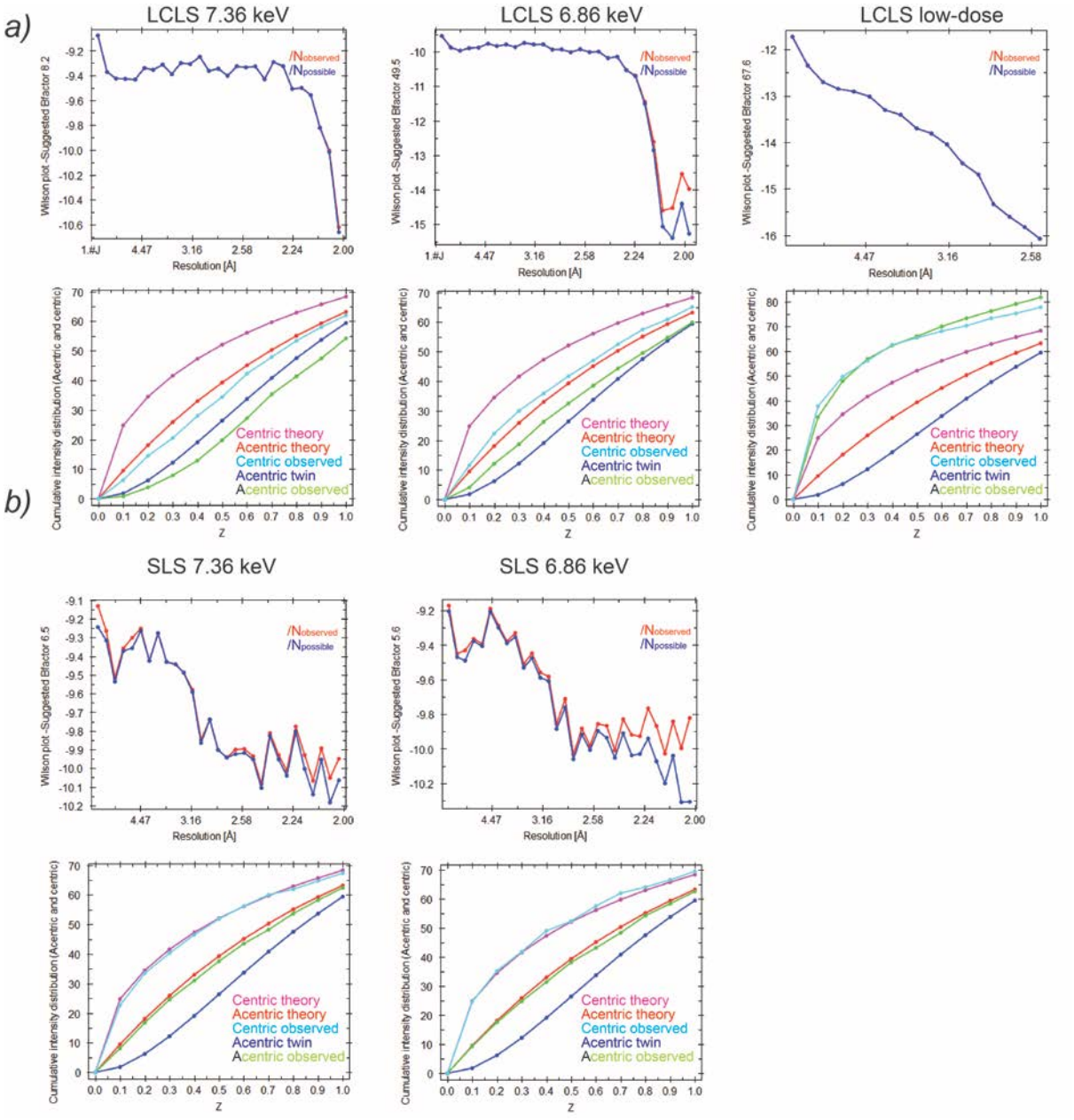

Figure S5 a) Ratios between ferredoxin structure factors calculated from a model with the coordinates of the two [4Fe-4S] clusters included and ferredoxin structure factors calculated of a model without the coordinates of the two [4Fe-4S] clusters (red) that are 10 or more times higher in magnitude. Ratios between structure factors measured at the synchrotron and at the LCLS at 7.36 keV (green). Ratios of the two ratios (blue).

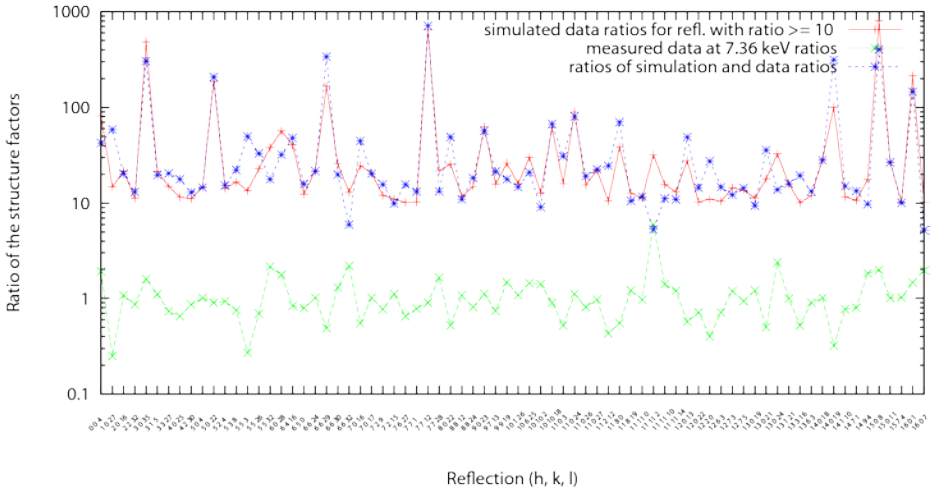

b) Ratios of the calculated ferredoxin structure factors from models with the coordinates of the two [4Fe-4S] clusters included and without the coordinates of the two [4Fe-4S] clusters, chosen at random (red). Ratios between structure factors measured at the synchrotron and at the LCLS at 7.36 keV (green). Ratios of the two ratios (blue).

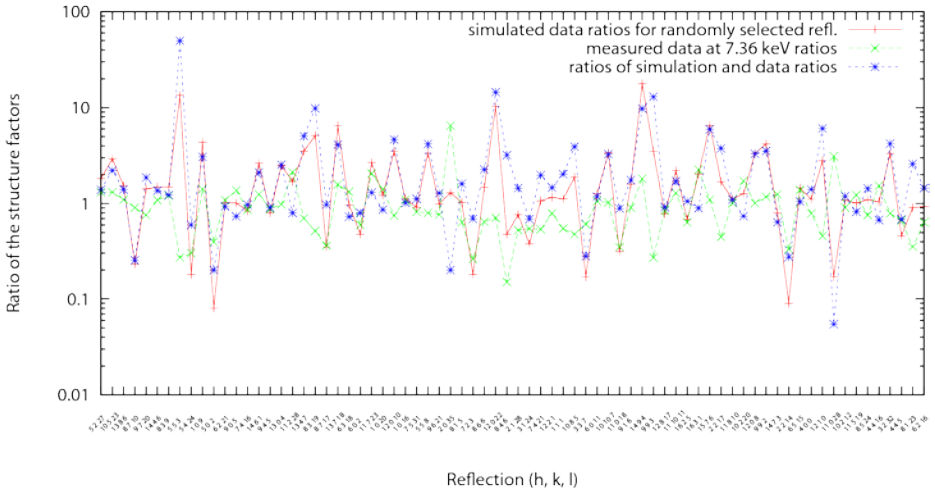

Figure S6 Simulation of Bragg termination. Wilson plots and cumulative intensity distributions for unaltered synchrotron data (a,b) as well as for the same data modified according to formula 3 from (Barty *et al.*, 2012) assuming 10 Å (c, d) and 40 Å (e, f) atomic displacement at the end of the pulse. Neither the unusual Wilson plots, nor the unusual cumulative intensity distributions observed for the LCLS ferredoxin data are reproduced by Bragg termination alone. For 40 Å atomic displacement, the cumulative intensity distribution has even moved in the opposite direction of what is observed in the LCLS data.

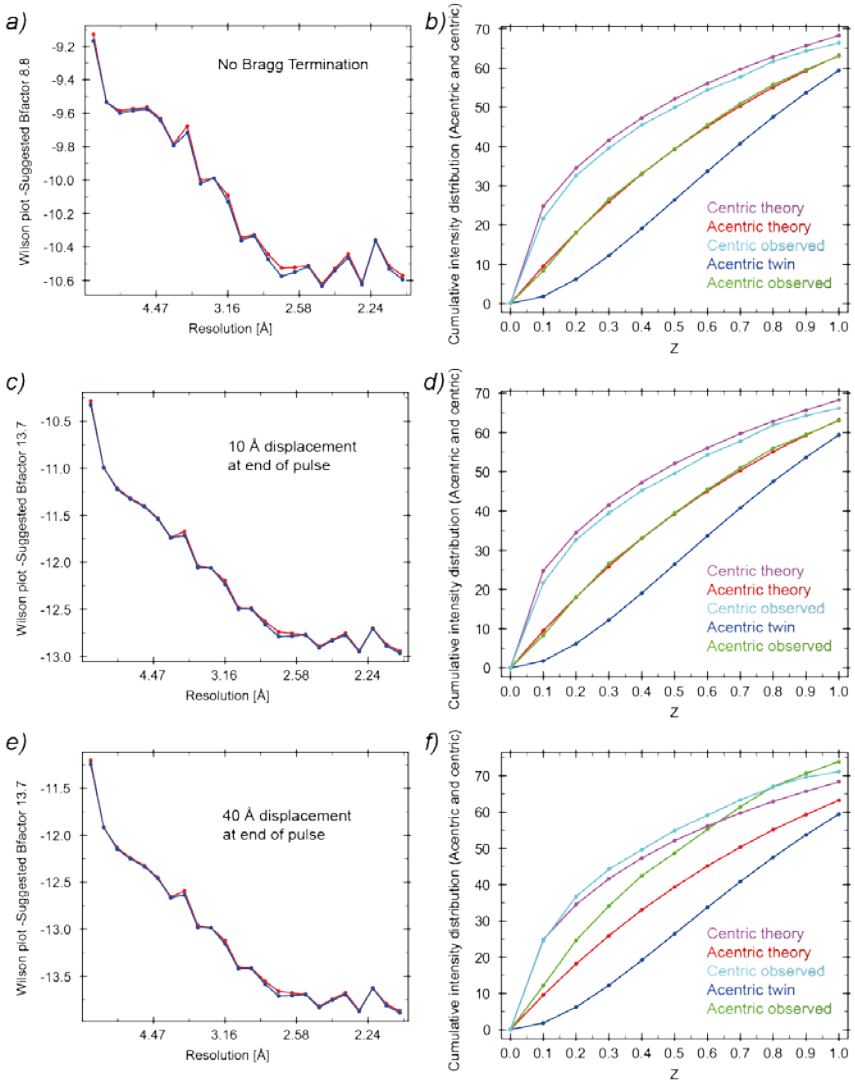

Figure S7 Simulation of Bragg termination with random local damage to different crystals reproduces the experimental intensity distribution.

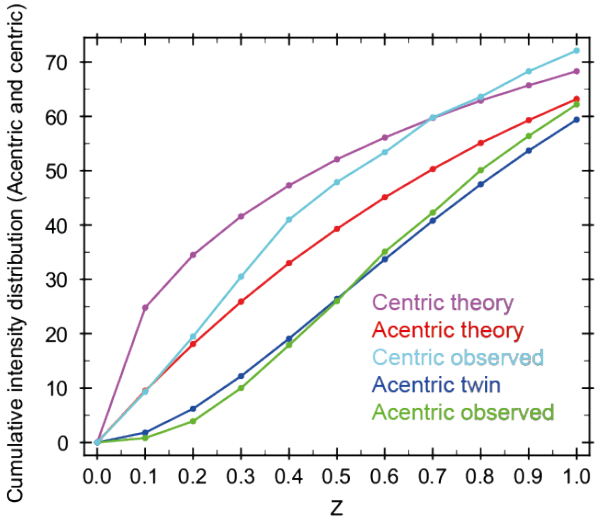

Figure S8 Information contents of the SLS and LCLS datasets collected above the Fe K-edge. $2mF_{obs}$ - DF_{calc} map (1 σ, blue) F_{obs} - DF_{calc} (3 σ, green) electron density maps calculated after simulated annealing using PHENIX of the published ferredoxin model (2FDN, (Dauter *et al.*, 1997)) after removal of tyrosine 30, against the a) the high dose LCLS data, b) the low dose LCLS data, and c) the SLS data. Very little density for the missing residue (displayed for reference) returns in the high dose LCLS electron density map (a), whereas it is reasonably well and very well defined in the low dose LCLS (b) and SLS maps (c), respectively. The same feature is observed when omitting other amino acids.

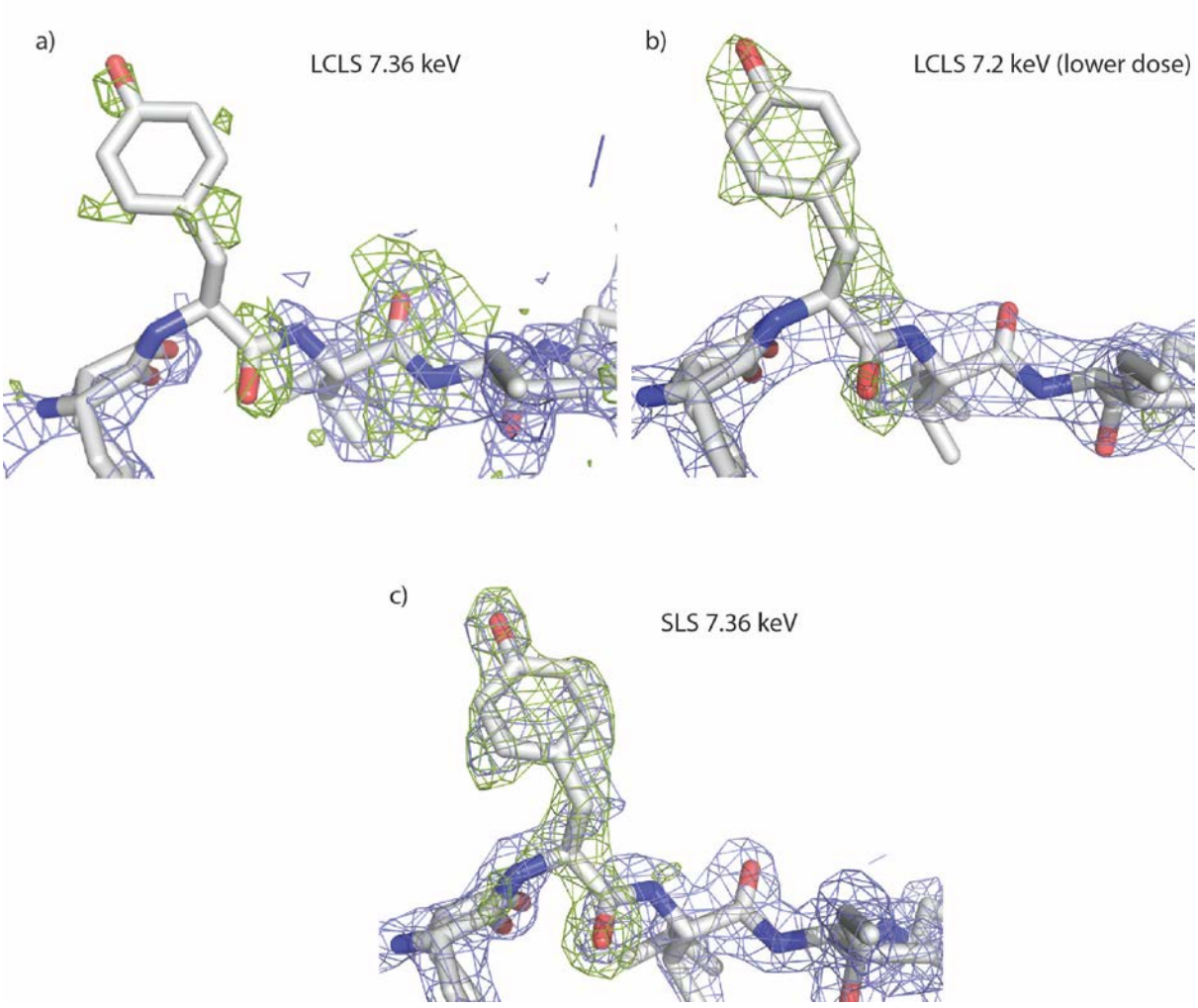

S1. Anomalous signal and phasing

Iron has a strong anomalous signal at 7.36 keV. We calculated phased anomalous difference Fourier maps from the LCLS data set. Fig. S9 shows the anomalous difference density peaks around iron atoms for the 7.36 keV LCLS data set contoured at 3σ and 5σ respectively. The heights of the anomalous peaks around Fe atoms in cluster 1 and cluster 2 are similar.

Phasing of the 7.36 keV synchrotron data by the single wavelength anomalous diffraction (SAD) approach was straightforward using the program Phaser (McCoy *et al.*, 2007) followed by automatic model building using ARP/wARP. However, neither this approach nor a slightly modified version of the one described by Barends *et al*. for the *de-novo* phasing of SFX data of a lysozyme gadolinium derivative (Barends *et al.*, 2013) was successful for the ferredoxin SFX data. This is in line with the relatively low CC_{ano} (0.18) of the FEL data set. We next tried phasing by applying a single isomorphous replacement (SIR) approach, using the synchrotron data as native dataset and the 7.4 keV SFX data as derivative, analogously to a radiation damage-induced phasing (RIP) approach. However, also in this case it was not possible to phase the data, likely due to an apparent non-isomorphism of the two datasets caused by the unusual intensity distribution described in Section 3.1. Given the relative ease of phasing the synchrotron data using the anomalous signal of iron, and the difficulty in phasing the SFX structure using the same approach, it is quite likely that this is due to the difference of the data quality of the two data sets.

Figure S9 Phased anomalous difference Fourier map from LCLS high dose 7.36 keV data set contoured at 3 σ (a) and 5 σ (b). The heights of the peaks around the Fe atoms in cluster 1 and cluster 2 are similar.

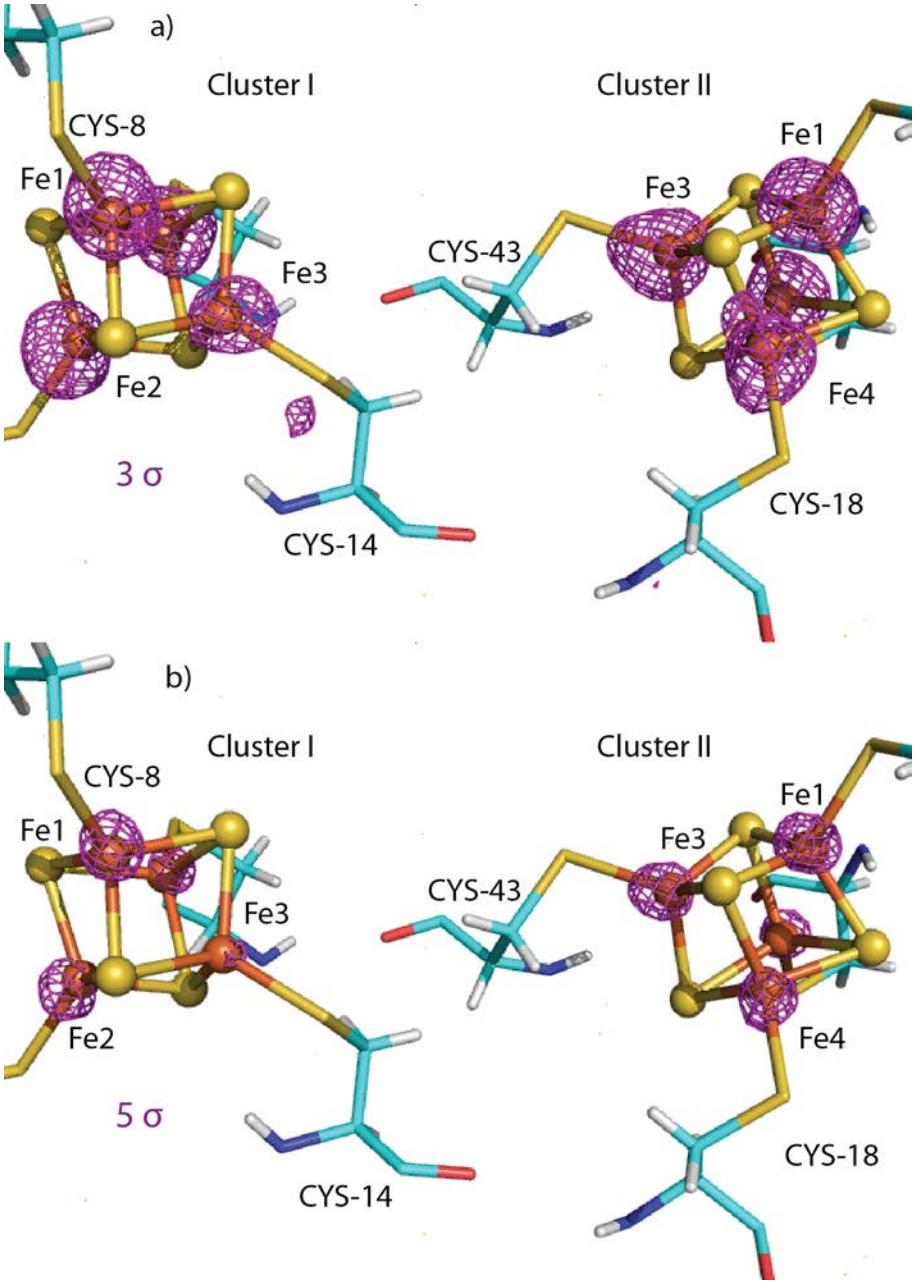

Figure S10 a) Difference electron density maps between the 7.36 keV LCLS and 6.86 keV LCLS high dose data sets at ± 3 σ (green/red). No significant difference electron density is apparent around the cluster atoms. The sulphur atoms in the cysteine residues that hold the clusters in place have significant positive difference density. In particular residues 8, 14, 37 and 43. b) The same view for corresponding maps calculated with the SLS data, showing noise peaks not associated with atomic positions.

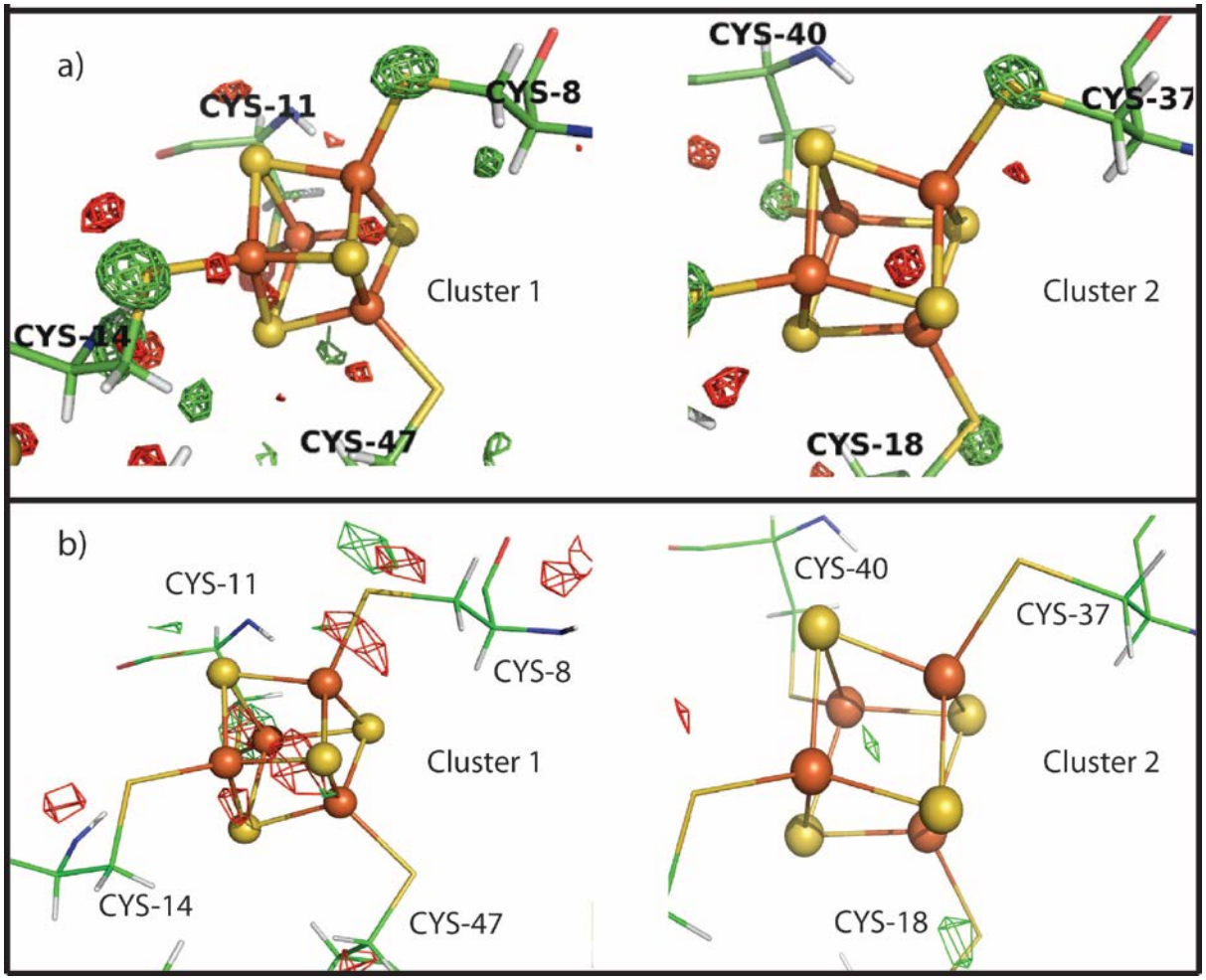

Figure S11 Structure of the ferredoxin molecule solved to 0.94 Å resolution from data collected at 100 K by (Dauter *et al.*, 1997). Cluster 1 is in the vicinity of the "mobile loop" (residues 26-28). Coloring according to B-factor values.

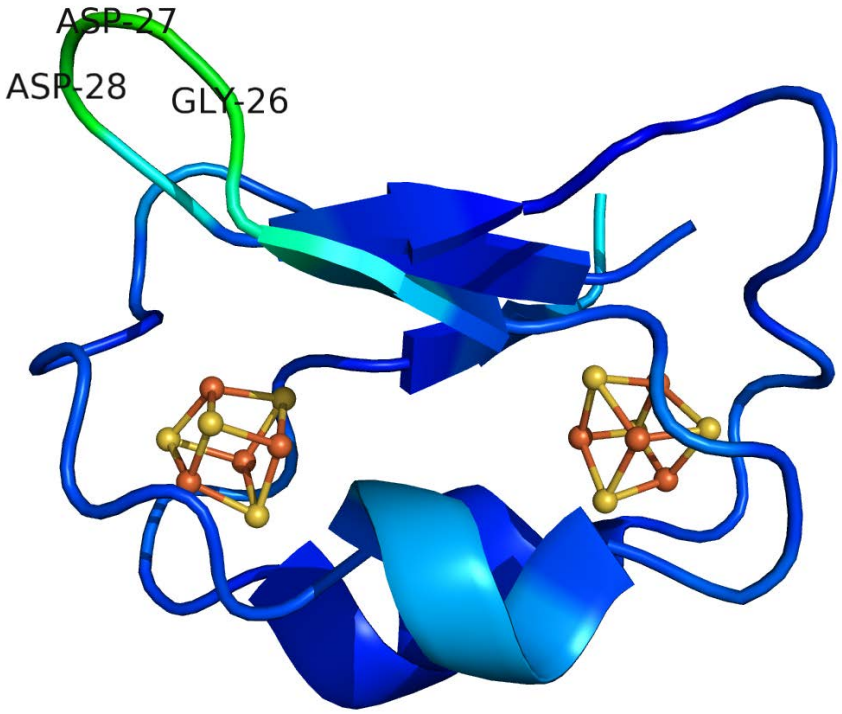

S2. Scaling

The LCLS and SLS data sets were scaled with XSCALE from XDS package. The summarized outputs from XSCALE and from the "Isomorphous difference map" tool in Phenix are given in table S1. Numbers in parentheses refer to the highest resolution shell.

Table S1 Summarized scaling statistics.

SLS and LCLS data sets	**7.36 keV[1]**	**6.86 keV[1]**
CC (XSCALE)	**0.85**	**0.86**
R-factor (XSCALE)	**0.38 (0.77)**	**0.40 (1.10)**
CC (PHENIX)	**0.83 (0.64)**	**0.67 (0.12)**
R-factor (PHENIX)	**0.26 (0.33)**	**0.30 (1.35)**
LCLS low dose and LCLS high dose data sets	**7.2 & 7.36 keV**	**7.2 & 6.86 keV**
CC (XSCALE)	**0.88**	**0.87**
R-factor (XSCALE)	**0.40 (0.67)**	**0.31 (0.56)**
CC (PHENIX)	**0.83 (0.68)**	**0.82 (0.66)**
R-factor (PHENIX)	**0.31 (0.38)**	**0.29 (0.36)**
LCLS low dose and SLS data sets	**7.2 & 7.36 keV**	**7.2 & 7.36 keV**
CC (XSCALE)	**0.94**	**0.96**
R-factor (XSCALE)	**0.22 (0.86)**	**0.23 (0.81)**
CC (PHENIX)	**0.88 (0.74)**	**0.89 (0.75)**
R-factor (PHENIX)	**0.19 (0.32)**	**0.19 (0.31)**

[1] Resolution range as mentioned in Table 1.

Table S2 R-factors for intensities of the low dose 7.2 keV LCLS data set from XSCALE scaled to 7.36 keV SLS RT data set.

RESOLUTION	R-FACTOR observed	R-FACTOR expected
10.00	23.6%	12.1%
8.00	9.5%	12.5%
7.00	21.4%	13.0%
6.00	19.6%	12.9%
4.50	12.8%	14.9%
4.00	13.6%	15.2%
3.50	15.8%	17.9%
3.00	17.5%	21.3%
2.90	19.3%	26.3%
2.80	34.6%	35.0%
2.70	49.3%	56.6%
2.60	62.4%	66.5%
2.50	86.2%	92.3%
total	22.5%	24.0%

Table S3 R-factors for intensities of the low dose 7.2 keV LCLS data set from XSCALE scaled to the 7.36 keV LCLS high dose data set.

RESOLUTION LIMIT	R-FACTOR observed	R-FACTOR expected
10.00	42.0%	34.4%
8.00	44.0%	35.1%
7.00	30.0%	33.4%
6.00	35.1%	33.7%
4.50	38.4%	34.7%
4.00	39.1%	34.7%
3.50	43.4%	35.3%
3.00	34.7%	34.8%
2.90	36.9%	36.3%
2.80	36.6%	37.2%
2.70	40.2%	46.4%
2.60	51.4%	52.5%
2.50	67.4%	64.2%
total	40.3%	37.3%

Table S4 R-factors for intensities of the high dose 7.36 keV LCLS data set from XSCALE scaled to the 7.36 keV SLS RT data set.

RESOLUTION LIMIT	R-FACTOR observed	R-FACTOR expected
10.00	41.6%	28.5%
8.00	41.5%	27.8%
7.00	47.8%	28.8%
6.00	44.8%	30.1%
4.50	33.8%	29.2%
4.00	35.1%	29.1%
3.50	35.6%	30.1%
3.00	32.9%	31.8%
2.50	35.1%	33.6%
2.30	35.5%	35.3%
2.20	34.3%	39.0%
2.10	36.7%	51.6%
2.00	76.8%	105.8%
total	37.6%	36.5%

Table S5 R-factors for intensities of the high dose 6.86 keV LCLS data set from XSCALE scaled to the 6.86 keV SLS RT data set.

RESOLUTION LIMIT	R-FACTOR observed	R-FACTOR expected
10.00	42.3%	29.3%
8.00	45.0%	29.5%
7.00	48.0%	30.3%
6.00	48.2%	38.0%
4.50	33.7%	30.6%
4.00	37.0%	31.3%
3.50	35.9%	33.4%
3.00	32.0%	33.2%
2.50	35.0%	37.0%
2.30	39.5%	42.6%
2.20	59.8%	72.1%
2.10	109.5%	102.8%
total	39.7%	38.8%

Table S6 Scaling statistics of the 7.36 keV LCLS high dose and SLS RT data sets using Phenix

Bin#	Resolution range	Completeness	No. of reflections	CC	R factor
1:	15.1833 - 3.6214	0.97	588	0.908	0.2570
2:	3.6214 - 2.8808	0.97	549	0.896	0.2364
3:	2.8808 - 2.5185	0.97	530	0.843	0.2364
4:	2.5185 - 2.2891	0.97	518	0.823	0.2548
5:	2.2891 - 2.1255	0.97	501	0.854	0.2449
6:	2.1255 - 2.0005	0.97	467	0.645	0.3274

Table S7 Scaling statistics of the 6.86 keV LCLS high dose and SLS RT data sets using Phenix

Bin#	Resolution range	Completeness	No. of reflections	CC	R-factor
1:	15.4585 - 3.6230	0.86	589	0.914	0.2505
2:	3.6230 - 2.8818	0.86	535	0.867	0.2362
3:	2.8818 - 2.5193	0.86	518	0.797	0.2652
4:	2.5193 - 2.2897	0.86	492	0.811	0.2565
5:	2.2897 - 2.1261	0.86	434	0.548	0.4341
6:	2.1261 - 2.0010	0.86	230	0.118	1.3552

Table S8 Scaling statistics of the 7.2 keV LCLS low dose and 6.86 keV SLS RT data sets using Phenix

Bin#	Resolution range	Completeness	No. of reflections	CC	R-factor
1:	17.2961 - 3.5990	0.97	601	0.951	0.1313
2:	3.5990 - 2.8608	0.97	548	0.965	0.1210
3:	2.8608 - 2.5004	0.97	535	0.754	0.3127

Table S9 Scaling statistics from the LCLS high dose 6.86 keV and LCLS high dose data sets at 6.86 keV from Phenix:

Bin#	Resolution range	Completeness	No. of reflections	CC	R-factor
1:	30.9185 - 3.6049	1.00	622	0.890	0.2623
2:	3.6049 - 2.8620	1.00	564	0.903	0.2561
3:	2.8620 - 2.5004	1.00	557	0.664	0.3591

Table S10 Integration of the *m*Fo-DFc density of the two iron-sulphur clusters for the different data sets. The electron density in all voxels around a cluster was summed up to obtain these numbers.

Dataset	cluster 2	cluster 1	Ratio 2:1
LCLS, 7.36 keV	1172	842	1.4
LCLS, 6.86 keV	1037	932	1.1
LCLS, 7.23 keV low dose	1701	1209	1.4
SLS, RT, 7.36 keV	1022	981	1.0
SLS, RT, 6.86 keV	1110	1054	1.1

S3. Difference map calculations

The ferredoxin crystal used in this study show a distribution of unit cell constants. While SFX datasets using the same batch of microcrystals will have the same widths of distributions, averaging out non-isomorphism effects, this is not the case when comparing data of single crystals. Because of a possible non-isomorphism between single crystals used for data collection at the synchrotron as well as between these crystals and the SFX microcrystal batches, calculation of a Fobs (crystal1) – Fobs (crystal2) difference electron density may not be meaningful. As shown in figure S12 a below, there is significant difference electron density around cluster 1 in the map calculated of the scaled 7.36 keV SLS and 6.86 keV SLS data sets, significant difference density is visible close to but not at the cluster 1 atomic positions. This is likely caused by non-isomorphism. In order to address this issue, we superposed the $2mF_{obs}$-DF_{calc} electron density maps in Phenix.superpose_maps and then calculated a difference map using MAPMAN from CCP4. Figure S12 b shows the difference map after this procedure. The difference peaks around cluster 1 disappeared, in line with a non-isomorphism between two crystals (see Table 1 for their unit cell parameters).

Because there is a distribution in the unit cell parameters of the SFX data (see Supplement Fig. S3) it could be possible that the peaks in the difference map in Fig. 4 were caused by non-isomorphism as well. However, when superimposing the $2mF_{obs}$-DF_{calc} maps calculated using the SLS and high dose LCLS data before subtracting them, the same result was obtained as shown in Fig. 4. This strongly supports that the difference are caused by radiation damage and not by non-isomorphism.

Figure S12 Difference electron density maps F_{obs}(SLS 7.36 keV) -F_{obs}(SLS 6.86 keV) contoured at ± 3 σ (positive – green mesh, negative – red mesh). a) calculated after scaling shows difference density around cluster 1 (left). b) calculated after scaling and superposing $2mF_{obs}$-DF_{calc} maps before calculating their difference, shows no difference density around cluster 1 (left.)

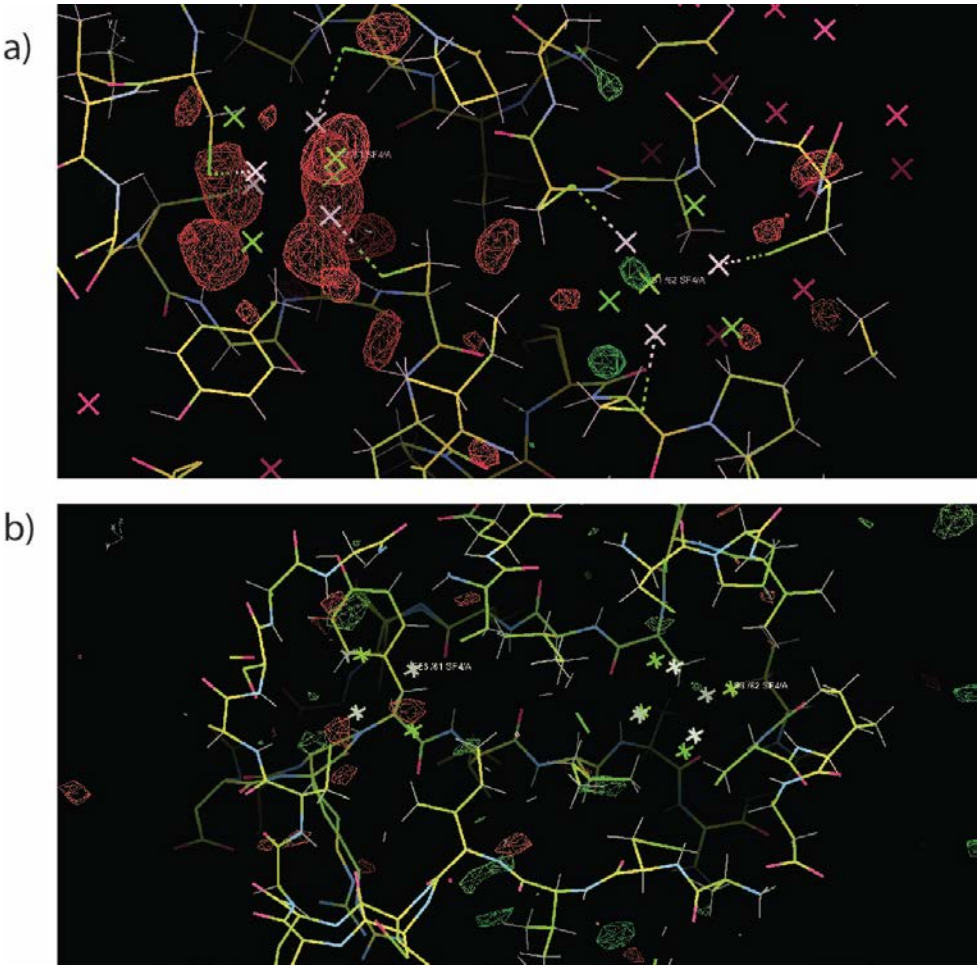

Table S11 Data statistics from CrystFEL for the LCLS high dose 7.36 keV data set. a) R_{split}, b) CC, c) CC*, d) R_{ano}/R_{split}, e) CC_{ano}, f) Redundancy, SNR and other data statistics.

a)

Resolution shell centre (1/nm)	R_{split} (%)	No. of reflections	Resolution shell centre (Å)
1.295	7.80	585	7.72
2.623	8.85	567	3.81
3.136	10.70	586	3.19
3.516	11.40	573	2.84
3.827	13.33	567	2.61
4.093	13.55	578	2.44
4.328	14.35	559	2.31
4.541	19.16	570	2.20
4.735	33.13	569	2.11
4.914	62.02	533	2.04

b)

Resolution shell centre (1/nm)	CC	No. of reflections	Resolution shell centre (Å)
1.295	0.97113	585	7.72
2.623	0.96169	567	3.81
3.136	0.93454	586	3.19
3.516	0.92733	573	2.84
3.827	0.90447	567	2.61
4.093	0.92329	578	2.44
4.328	0.90125	559	2.31
4.541	0.87942	570	2.20
4.735	0.53172	569	2.11
4.914	0.29073	533	2.04

c)

Resolution shell centre (1/nm)	CC*	No. of reflections	Resolution shell centre (Å)
1.295	0.99265	585	7.72
2.623	0.99018	567	3.81
3.136	0.98293	586	3.19
3.516	0.98096	573	2.84
3.827	0.97459	567	2.61
4.093	0.97985	578	2.44
4.328	0.97368	559	2.31
4.541	0.96739	570	2.20
4.735	0.83323	569	2.11
4.914	0.67119	533	2.04

d)

Resolution shell centre (1/nm)	R_{ano} / R_{split}	No. of reflections	Resolution shell centre (Å)
1.503	1.46326	386	6.65
2.635	1.28121	444	3.79
3.143	1.33504	482	3.18
3.521	1.33955	486	2.84
3.830	1.39174	478	2.61
4.096	1.28597	496	2.44
4.330	1.19681	486	2.31
4.542	1.16798	498	2.20
4.735	1.12122	502	2.11
4.914	1.03139	462	2.04

e)

Resolution shell centre (1/nm)	CC_{ano}	No. of reflections	Resolution shell centre (Å)
1.503	0.31425	386	6.65
2.635	0.22138	444	3.79
3.143	0.27964	482	3.18
3.521	0.24415	486	2.84
3.830	0.22270	478	2.61
4.096	0.31139	496	2.44
4.330	0.19900	486	2.31
4.542	0.17169	498	2.20
4.735	-0.00699	502	2.11
4.914	-0.09042	462	2.04

f)

1/d (1/nm)	No. of reflections	Possible	Compl. (%)	No. of measurements	Red.	SNR	d (Å)
1.295	585	585	100.00	272675	466.1	15.50	7.72
2.623	567	567	100.00	271762	479.3	13.08	3.81
3.136	586	586	100.00	269278	459.5	11.40	3.19
3.516	573	573	100.00	277800	484.8	10.15	2.84
3.827	567	567	100.00	255837	451.2	8.79	2.61
4.093	578	578	100.00	268379	464.3	8.28	2.44
4.328	559	559	100.00	268399	480.1	7.79	2.31
4.541	570	570	100.00	197583	346.6	6.06	2.20
4.735	570	570	100.00	117087	205.4	4.09	2.11
4.914	562	565	99.47	82905	147.5	2.27	2.04

Table S12 Data statistics from CrystFEL for the LCLS high dose 6.86 keV data set. a) R_split, b) CC, c) CC*, d) Redundancy, SNR and other data statistics

a)

Resolution shell centre (1/nm)	R_{split} (%)	No. of reflections	Resolution shell centre (Å)
1.240	11.08	501	8.06
2.499	14.40	502	4.00
2.987	14.20	487	3.35
3.349	18.01	487	2.99
3.644	20.84	500	2.74
3.898	21.44	495	2.57
4.122	26.70	497	2.43
4.325	37.84	476	2.31
4.509	56.53	439	2.22
4.680	101.38	343	2.14

b)

Resolution shell centre (1/nm)	CC	No. of reflections	Resolution shell centre (Å)
1.240	0.94665	501	8.06
2.499	0.88626	502	4.00
2.987	0.90317	487	3.35
3.349	0.85817	487	2.99
3.644	0.79086	500	2.74
3.898	0.83373	495	2.57
4.122	0.75911	497	2.43
4.325	0.53572	476	2.31
4.509	0.52997	439	2.22
4.680	0.27790	343	2.14

c)

Resolution shell centre (1/nm)	CC*	No. of reflections	Resolution shell centre (Å)
1.240	0.98620	501	8.06
2.499	0.96938	502	4.00
2.987	0.97422	487	3.35
3.349	0.96108	487	2.99
3.644	0.93980	500	2.74
3.898	0.95358	495	2.57
4.122	0.92901	497	2.43
4.325	0.83527	476	2.31
4.509	0.83233	439	2.22
4.680	0.65949	343	2.14

d)

1/d (1/nm)	No. of reflections	Possible	Compl (%)	No. of measurements	Red.	SNR	d (Å)
1.239	506	506	100.00	106698	210.9	10.2	8.07
2.498	503	503	100.00	102345	203.5	8.53	4.00
2.987	487	487	100.00	102713	210.9	7.71	3.35
3.349	487	487	100.00	101649	208.7	6.68	2.99
3.644	500	500	100.00	97531	195.1	5.65	2.74
3.898	495	495	100.00	106837	215.8	5.25	2.57
4.122	498	498	100.00	98506	197.8	4.64	2.43
4.325	479	479	100.00	62053	129.5	3.35	2.31
4.509	487	500	97.40	38093	78.2	1.97	2.22
4.680	415	485	85.57	23885	57.6	0.52	2.14

Table S13 Data statistics from CrystFEL for the LCLS low dose 7.2 keV data set. a) R_{split}, b) CC, c) CC*, d) CC_ano, e) Redundancy, SNR and other data statistics.

a)

Resolution shell centre (1/nm)	R_{split} (%)	No. of reflections	Resolution shell centre (Å)
1.062	9.29	227	9.42
2.099	12.05	195	4.76
2.509	14.68	188	3.99
2.813	17.50	183	3.55
3.061	21.82	178	3.27
3.275	22.03	179	3.05
3.463	28.16	179	2.89
3.633	64.52	170	2.75
3.788	79.65	177	2.64
3.931	107.45	161	2.54

b)

Resolution shell centre (1/nm)	CC	No. of reflections	Resolution shell centre (Å)
1.062	0.9887265	227	9.42
2.099	0.9679361	195	4.76
2.509	0.9592102	188	3.99
2.813	0.9426913	183	3.55
3.061	0.8939354	178	3.27
3.275	0.9257103	179	3.05
3.463	0.8911672	179	2.89
3.633	0.4493055	170	2.75
3.788	0.4276729	177	2.64
3.931	0.3388836	161	2.54

c)

Resolution shell centre (1/nm)	CC*	No. of reflections	Resolution shell centre (Å)
1.062	0.9971616	227	9.42
2.099	0.9918200	195	4.76
2.509	0.9895355	188	3.99
2.813	0.9851398	183	3.55
3.061	0.9715955	178	3.27
3.275	0.9805214	179	3.05
3.463	0.9707997	179	2.89
3.633	0.7874190	170	2.75
3.788	0.7740277	177	2.64
3.931	0.7114901	161	2.54

d)

Resolution shell centre (1/nm)	CCano	No. of reflections	Resolution shell centre (Å)
1.062	0.4842724	227	9.42
2.099	0.1148118	195	4.76
2.509	0.2819113	188	3.99
2.813	0.0124190	183	3.55
3.061	0.1726478	178	3.27
3.275	0.2571544	179	3.05
3.463	0.0195008	179	2.89
3.633	0.1253152	170	2.75
3.788	0.0020382	177	2.64
3.931	0.000000	161	2.54

e)

1/d (1/nm)	No. of reflections	Possible	Compl (%)	No. of measurements	Red.	SNR	d (Å)
1.062	227	227	100.00	57136	251.7	10.08	9.42
2.099	195	195	100.00	47348	242.8	7.68	4.76
2.509	188	188	100.00	46025	244.8	6.76	3.99
2.813	183	183	100.00	43538	237.9	5.21	3.55
3.061	178	178	100.00	44208	248.4	5.20	3.27
3.275	179	179	100.00	45886	256.3	4.02	3.05
3.463	179	179	100.00	38152	213.1	3.13	2.89
3.633	170	170	100.00	25973	152.8	1.83	2.75
3.788	178	178	100.00	19373	108.8	1.42	2.64
3.931	162	163	99.39	12866	79.4	0.99	2.54

Supplementary references

Barends, T. R., Foucar, L., Shoeman, R. L., Bari, S., Epp, S. W., Hartmann, R., Hauser, G., Huth, M., Kieser, C., Lomb, L., Motomura, K., Nagaya, K., Schmidt, C., Strecker, R., Anielski, D., Boll, R., Erk, B., Fukuzawa, H., Hartmann, E., Hatsui, T., Holl, P., Inubushi, Y., Ishikawa, T., Kassemeyer, S., Kaiser, C., Koeck, F., Kunishima, N., Kurka, M., Rolles, D., Rudek, B., Rudenko, A., Sato, T., Schroeter, C. D., Soltau, H., Strueder, L., Tanaka, T., Togashi, T., Tono, K., Ullrich, J., Yase, S., Wada, S. I., Yao, M., Yabashi, M., Ueda, K. & Schlichting, I. (2013). *Acta Crystallogr.D.Biol.Crystallogr.* **69**, 838-842.

Barty, A., Caleman, C., Aquila, A., Timneanu, N., Lomb, L., White, T. A., Andreasson, J., Arnlund, D., Bajt, S., Barends, T. R., Barthelmess, M., Bogan, M. J., Bostedt, C., Bozek, J. D., Coffee, R., Coppola, N., Davidsson, J., DePonte, D. P., Doak, R. B., Ekeberg, T., Elser, V., Epp, S. W., Erk, B., Fleckenstein, H., Foucar, L., Fromme, P., Graafsma, H., Gumprecht, L., Hajdu, J., Hampton, C. Y., Hartmann, R., Hartmann, A., Hauser, G., Hirsemann, H., Holl, P., Hunter, M. S., Johansson, L., Kassemeyer, S., Kimmel, N., Kirian, R. A., Liang, M., Maia, F. R., Malmerberg, E., Marchesini, S., Martin, A. V., Nass, K., Neutze, R., Reich, C., Rolles, D., Rudek, B., Rudenko, A., Scott, H., Schlichting, I., Schulz, J., Seibert, M. M., Shoeman, R. L., Sierra, R. G., Soltau, H., Spence, J. C., Stellato, F., Stern, S., Struder, L., Ullrich, J., Wang, X., Weidenspointner, G., Weierstall, U., Wunderer, C. B. & Chapman, H. N. (2012). *Nat.Photonics.* **6**, 35-40.

Dauter, Z., Wilson, K. S., Sieker, L. C., Meyer, J. & Moulis, J. M. (1997). *Biochemistry* **36**, 16065-16073.

Krumrey, M. & Ulm, G. (2001). *Nuclear Instruments and Methods in Physics Research Section A: Accelerators, Spectrometers, Detectors and Associated Equipment* **467–468, Part 2**, 1175-1178.

McCoy, A. J., Grosse-Kunstleve, R. W., Adams, P. D., Winn, M. D., Storoni, L. C. & Read, R. J. (2007). *Journal of applied crystallography* **40**, 658-674.